7-2002

Sensitivity Comparison of Ladar Receivers Designed to Detect Glint Targets

Christopher D. Brewer
University of Dayton

Bradley D. Duncan
University of Dayton, bduncan1@udayton.edu

Edward A. Watson
Wright Laboratory

Sensitivity comparison of ladar receivers designed to detect glint targets

Christopher D. Brewer
Bradley D. Duncan, MEMBER SPIE
University of Dayton
Center for Electro-Optics
300 College Park
Dayton, Ohio 45469-0245
E-mail: Bradley.Duncan@notes.udayton.edu

Edward A. Watson, FELLOW SPIE
Air Force Wright Laboratory
EO Sensor Technology Branch
3109 P Street
Wright Patterson AFB, Ohio 45433-7700

Abstract. We present four receiver designs for a ladar system, based on an optical parametric amplifier, that is designed to collect returns from glint targets. After coupling the return energy into periodically poled lithium niobate, the target backscatter is detected with either an infrared camera or a CCD array. Assuming reasonable detector and system characteristics, the sensitivity of each design is then evaluated by setting the receiver SNR detection threshold equal to one and using the minimum transmitted energy as the figure of merit. Through numerical analysis, we show that an upconversion receiver followed by a visible CCD array offers the best trade-off between sensitivity and practical design for airborne ladar applications. [DOI: 10.1117/1.1479709]

Subject terms: glint targets; ladar; image upconversion.

Paper 010124 received Apr. 4, 2001; revised manuscript received Dec. 19, 2001; accepted for publication Jan. 11, 2002.

1 Introduction

Over the past several years, a great deal of work has been sponsored by the United States Air Force to develop various types of ladar (laser detection and ranging) systems. Similar to conventional radar systems, the most basic purpose of a pulsed ladar system is to illuminate a target with a laser beam and then collect and focus as much return energy as possible onto a detector. By measuring the time difference between the transmitted and received pulses, the range to the object or a specific point on the object can be determined. By then scanning the beam across a target and measuring the time differential at each point, a ladar system can build up a one-, two-, or three-dimensional image with a modest amount of postdetection processing.

Besides the ability to detect and range targets, most state-of-the-art ladar systems are also designed to operate at a wavelength that is eyesafe. For a system to be deemed eyesafe under normal operating conditions, the lens, aqueous humor, and cornea of the eye must absorb the laser radiation before the retina is damaged. This requirement limits the source wavelength to the infrared region (1.4 to 1000 μm) of the spectrum.[1] As a result, several studies using infrared (IR) source wavelengths are currently underway.[2]

One such IR source under investigation is the optical parametric oscillator (OPO). By pumping a nonlinear crystal such as lithium niobate ($LiNbO_3$) with an infrared source of wavelength λ_p, two separate eye-safe beams can be generated through difference-frequency generation (DFG).[3] If the pump wavelength, the temperature, or the orientation of the OPO crystal inside the transmitter cavity is then varied, the output signal (λ_s) and idler (λ_i) wavelengths can be tuned to a spectral region where the target is highly reflective. However, constantly changing the pump or the crystal alignment is impractical, and the temperature tuning range is limited to a few microns.[3]

To overcome these difficulties, another OPO tuning technology, known as quasi-phase-matching (QPM), has been investigated.[4] Through QPM, a periodic grating structure is poled into a $LiNbO_3$ crystal and the output wavelengths tuned by varying the crystal temperature. The major advantage of QPM is that it is possible to pole a single crystal with several different grating structures, thereby expanding the tuning range to several microns of the IR spectrum.[5] This makes the OPO ladar system very attractive for multispectral target interrogation.

Aside from the increased operational wavelength range, periodically poled lithium niobate (PPLN) also permits the operator to enhance the cavity gain of the transmitter by accessing the largest element in the second-order nonlinear susceptibility tensor.[6] Even with this improvement, though, OPO-based ladar systems are inherently limited in the amount of energy available to illuminate a target. Typically PPLN transmitters can emit $\approx$1.0 mJ of signal energy per pulse before the damage threshold of the material is reached.[4] Depending on the atmospheric transmittance, the target reflectivity, and the range, by the time the return is focused onto a detector, the resulting power level may be well below the threshold necessary for reliable detection.[7] Since damage threshold imposes an upper limit on the transmitted power, the ladar designer is forced to modify the receiver to boost the magnitude of the target return.

It is with these issues in mind that we now investigate several different ladar system designs. Section 2 briefly outlines the properties of diffuse and glint targets and discusses how the return power from a glint target is determined. Once this is established, Sec. 3 examines the signal-to-noise ratios and minimum energy requirements of four different ladar receivers designed to detect glint targets. The four designs considered are a simple IR camera, an optical parametric amplifier (OPA) receiver, an upconver-

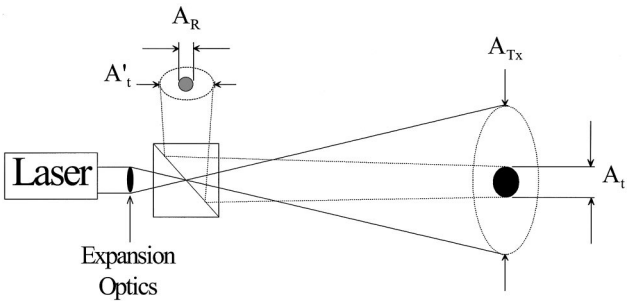

Fig. 1 Ladar geometry used to calculate the radiometric expressions for the received power.

sion receiver, and a receiver equipped with an image intensifier. We then present our conclusions in Sec. 4.

2 Power Received from a Glint Target

In general, ladar applications range from the remote sensing of hazardous gas clouds to detecting hard targets on a battlefield. For the purposes of this paper, our interest will focus solely on detecting hard objects. Whether the operator is interested in airborne or ground-based targets, all hard objects can be classified into two basic reflectivity categories: diffuse and glint.[8]

Diffuse targets ordinarily have very low reflectance. In addition, when illuminated, each subsurface across a diffuse target randomly scatters energy in a hemispherical region of space, with only a small fraction being directed back towards the receiver. The power received from various diffuse targets has recently been modeled by Steinvall.[9]

In contrast, a glint target is an object that scatters the return energy into a much narrower region of space. For example, on most man-made objects there are areas such as windows or bumpers that act like glint retroreflectors. Typically, power ratios from these types of targets are well over 100 : 1 with respect to a diffuse background.[10] Thus even though an OPO-based ladar system may be limited to low energies, it can still be used, for example, to search through dense ground cover for downed aircraft or other hidden targets. Once a glint object is found, the region can then be interrogated further to determine the true nature of the target. It is with this application in mind that we focus the remainder of this paper on evaluating several techniques for identifying glint targets against diffuse backgrounds.

To accomplish this task, a radiometric model describing the received power P_R from a flood-illuminated glint target is first developed. Since most glints are highly reflective in the retro direction, we will assume that the glint component from any surface can be adequately modeled as a corner-cube reflector with a circular cross section. Modeling the ladar system geometry as shown in Fig. 1, P_R is found by applying radiometric theory. Integrating the angularly dependent target radiance $L_t(\theta)$ over both the illuminated target area A_t and the solid angle Ω_R subtended by the receiver at the target, we find[11]

$$P_R = \int\int L_t(\theta)\, dA_t\, d\Omega_R. \tag{1}$$

Note that in formulating Eq. (1) the transmitter, target, and receiver planes are assumed to be parallel and centered with respect to one another, as shown in Fig. 1.

Equation (1) can now be simplified using basic radiometric definitions.[11] Relating the target-plane radiance $L_t(\theta)$ to the radiant exitance M, the total power per unit area reflected by the target can be written as

$$M = \frac{P_{Tx}\eta_{atm}^2\rho}{A_{Tx}} = \int L_t(\theta)\, d\Omega_t, \tag{2}$$

where P_{Tx} is the transmitted power, ρ is the angular reflectivity of the target, A_{Tx} is the area of the illumination beam in the target plane, and Ω_t is the *total* solid angle into which the light from the target radiates. Furthermore, η_{atm} is the wavelength-dependent atmospheric transmittance given by Beer's law,[12]

$$\eta_{atm}(\lambda, L) = \exp[-\gamma(\lambda)L], \tag{3}$$

where $\gamma(\lambda)$ is the spectral extinction coefficient and L is the target range. Note that this quantity is then squared in Eq. (2) to allow for the round-trip flight of the transmitted pulse. Because Ω_t is small for most glint targets, $L_t(\theta)$ is approximately constant and the integral in Eq. (2) reduces to

$$\frac{P_{Tx}\eta_{atm}^2\rho}{A_{Tx}} \approx L_t(\theta)\Omega_t. \tag{4}$$

If the target and receiver areas are both small with respect to the distance z by which they are separated, then solving Eq. (4) for $L_t(\theta)$ and substituting the result into Eq. (1) yields the following general expression for the received power:

$$P_R = P_{Tx}\rho\,\eta_{atm}^2\left(\frac{A_t}{A_{Tx}}\times\frac{\Omega_R}{\Omega_t}\right) = P_{Tx}\rho\,\eta_{atm}^2\left(\frac{A_t}{A_{Tx}}\times\frac{A_R}{A_t'}\right). \tag{5}$$

In this equation, $\Omega_R \approx A_R/z^2$, $\Omega_t \approx A_t'/z^2$, A_R is the receiver area, and A_t' is the area of the target's diffraction pattern in the receiver plane. From Eq. (5), we see that the received power is inversely proportional to the area of the target's diffraction pattern in the receiver plane. Unfortunately, once the geometry of the problem is established, unlike all the other variables in the expression, this one is not constant. Basic diffraction theory states that as the physical size of an object is decreased, diffraction becomes more pronounced, causing A_t' and the solid angle into which the target radiates to increase.[13]

To illustrate the implications of Eq. (5), consider the two limiting cases, which we refer to as the near-field and far-field regimes. As is typically the case, in both instances we assume that the target is in the far field with respect to the receiver (i.e., $z > 2D_R^2/\lambda_s$, where D_R is the receiver diameter).[13] In the near-field regime, then, the target area is assumed to be large enough that the receiver is in the target's near field (i.e., $z \ll 2D_t^2/\lambda_s$, where D_t is the target diameter). In this regime, diffraction effects in the receiver

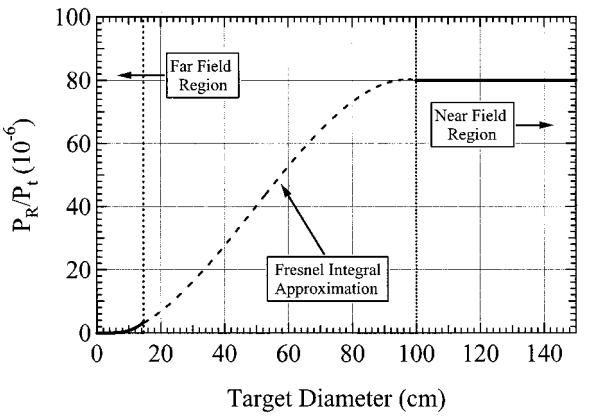

Fig. 2 Normalized received power versus target diameter. Here the target range is assumed to be 20 km, and Fresnel integrals have been used to approximate the region between the near-field and far-field boundaries.

plane are minimal, making $A_t \approx A_t'$. From Eq. (5), this causes P_R to remain constant with increasing target size. In contrast, in the far-field regime the target is small enough that the receiver is in the far field with respect to the target (i.e., $z \geqslant 2D_t^2/\lambda_s$), causing A_t' to expand due to diffraction.

With the glint object assumed to be circular, the target's far-field diffraction pattern in the receiver plane is readily found by applying Fraunhofer diffraction theory. Using the location of the first zeros in the Airy pattern to define the area $A_{t,ff}'$ of target's far field diffraction pattern, we find[13]

$$A_{t,ff}' = \pi\left(\frac{1.22\lambda_s z}{D_t}\right)^2 = \frac{(0.61\pi\lambda_s z)^2}{A_t}. \tag{6}$$

The total received power in each regime from a glint can then be summarized as follows:

$$P_R = P_{Tx}\rho\,\eta_{atm}^2\frac{A_R}{A_{Tx}}\begin{cases} 1, & [D_t \gg D_R], \\ A_t/A_t' & [\text{general case}], \\ A_t^2/(0.61\pi\lambda_s z)^2 & [D_t \leqslant (\lambda_s z/2)^{1/2}]. \end{cases} \tag{7}$$

The trends in Eq. (7) are understood more fully by plotting the normalized received power P_R/P_{Tx} versus target diameter as shown in Fig. 2. This figure was generated for a target range of 20 km using the reasonable ladar system parameters found in Table 1. In addition, we have assumed an eyesafe signal wavelength of $\lambda_s = 2.1\ \mu$m. At this wavelength, for a typical earth atmospheric, the transmittance is $\eta_{atm} \approx 0.97$ at 1 km and the value of the extinction coefficient in Eq. (3) is readily found to be $\gamma(\lambda) = 0.03/\text{km}$.[12] Given this reference point, η_{atm}^2 for a round trip of 20 km is approximately 29%. A Gaussian beam diameter of $2\omega_0 = 5.34$ mm was assumed at the exit aperture of the OPO transmitter. Once propagated to the target plane, this particular beam size produces a $1/e^2$ spot diameter of 10 m and flood-illuminates the object.

Upon inspection of Fig. 2, a few observations can be made. Recall that the near-field region nominally begins when the target diameter increases to the point where $D_t \gg D_R$. For the system parameters under consideration, then, we observe that the ratio of received to transmitted power becomes constant when $D_t \geqslant 1$ m. In addition, due to the A_t^2 in the far-field component of Eq. (7), the curve in Fig. 2 is quadratic below the far-field boundary. Given the system parameters in Table 1, this boundary occurs where the target diameter is equal to $D_t = 14.5$ cm. Furthermore, due to the division by z^2 in the far-field expression of Eq. (7), the received power is very small. This fact will present a challenge later: in keeping with the size of glint returns commonly observed in practice, beginning in Sec. 3 only glint target diameters less than 1 cm will be considered. For the ladar systems to be analyzed, however, this will make it possible to use exclusively the far-field diffraction model to determine the received power. Finally, in the dashed region between the two limiting cases, the glint diffraction pattern in the receiver plane transitions from an Airy pattern in the far field to roughly a mirror image of the target in the near field. Such a transformation is readily accounted for by numerically solving the Fresnel diffraction integral for a circular aperture,[13] but is beyond the scope of this paper.

Table 1 Parameters used to evaluate the effectiveness of the OPO-based ladar system and the various receiver designs.

Parameter	Symbol	Value
Transmitted pulse duration	$\Delta\tau$	1 ns
Transmitted beam diameter	$2\omega_0$	5.34 mm
OPO and SFG pump wavelength	λ_p	1.064 μm
Signal wavelength	λ_s	2.1 μm
Atmospheric extinction coefficient	$\gamma(\lambda)$	0.03/km
Target diameter	D_t	5 mm
Target reflectivity	ρ	0.8
Receiver diameter	D_R	10 cm

3 Receiver Designs

Having developed a model for the total power received from a glint target, we now examine how this information can be used to determine the minimum transmitted power needed to overcome detector noise. As stated earlier, typical ladar systems use standard optics to expand the transmitted beam and illuminate an object a distance z away. The light is then reflected off the target, collected by the receiver, and focused onto a detector. For a small glint target located in the far field with respect to the receiver, P_R from Eq. (7) can be written in terms of the transmitted signal energy E_{Tx} and the pulse duration $\Delta\tau$ as follows:

$$P_R = \frac{A_t^2 A_R \rho\,\eta_{atm}^2}{A_{Tx}(0.61\pi\lambda_s z)^2}\cdot P_{Tx} = C\left(\frac{E_{Tx}}{\Delta\tau}\right), \tag{8}$$

where

$$C = \frac{A_t^2 A_R \rho\,\eta_{atm}^2}{A_{Tx}(0.61\pi\lambda_s z)^2}. \tag{9}$$

Table 2 Infrared and CCD camera parameters used to evaluate the receiver signal-to-noise ratios.

Parameter	Symbol	Infrared camera	Visible CCD array
Responsivity	$\mathcal{R}$	0.89 A/W	0.48 A/W
Load resistance	R_L	50 Ω	5.1 kΩ
Dark current	I_D	100 nA	2 nA
Temperature	T_D	273 K	300 K

Depending on the transmitted energy, the illumination area, the type of target, the range, and the diameter of the receiver, the return power may be well below the system noise and never detected.

Choosing some reasonable values for the receiver characteristics, the effectiveness of the ladar receiver system can be evaluated. If these values are then held constant in each design, the various receiver configurations can be compared by analyzing the single-pixel signal-to-noise ratio at the detector (SNR_D). For this calculation, we have chosen as the figure of merit the minimum transmitter energy E_{Tx} needed to meet a detection threshold of $SNR_D = 1$. This threshold, however, is arbitrary and can be adjusted to meet the requirements of any given system.

As a baseline, consider a direct-detection ladar receiver with only an IR camera in the detector plane. Taking account of shot, dark current, and thermal noise, and assuming that the detector response time is much less than the transmitted pulse duration, the postdetection electrical signal-to-noise ratio for a single-pixel at the detector can be written as[14]

$$\mathrm{SNR_D}=\frac{P_{\mathrm{sig}}}{P_{\mathrm{shot}}+P_{\mathrm{thermal}}+P_{\mathrm{dark}}}$$

$$\mathrm{SNR_D}=\frac{(\mathcal{R}P_{\mathrm{R}})^2}{\frac{2q\mathcal{R}P_{\mathrm{R}}}{\Delta\tau}+\frac{2k_{\mathrm{b}}T_{\mathrm{D}}}{\Delta\tau R_{\mathrm{L}}}+\frac{2qI_{\mathrm{D}}}{\Delta\tau}} \quad , \qquad (10)$$

$$\mathrm{SNR_D}=\frac{(\mathcal{R}CE_{\mathrm{Tx}})^2}{2q\mathcal{R}CE_{\mathrm{Tx}}+2k_{\mathrm{b}}\Delta\tau T_{\mathrm{D}}/R_L+2q\Delta\tau I_{\mathrm{D}}}$$

where $\mathcal{R}$ is the detector responsivity, q is the charge of the electron, and k_b is Boltzmann's constant. Likewise T_D is the temperature of the detector in kelvins, R_L is the equivalent load resistance, and I_D is the dark current. This expression assumes that all of the received power is focused onto the detector.

Employing the ladar system parameters in Table 1 and the example detector parameters from a Sensors Unlimited SU128-1.7 RT infrared camera (Table 2), we can calculate the minimum transmitted pulse energy for $SNR_D = 1$ at various target ranges. This trend is displayed in Fig. 3 for the simple IR camera receiver, as well as the other receiver designs to be examined shortly. As expected, to ensure the same level of detection, we see that E_{Tx} must increase as the target range increases. In addition, to examine how the glint target reflectivity affects the receiver sensitivity, we once again set the $SNR_D = 1$ in Eq. (10) and solve for the minimum transmitted energy at a fixed target range $L = 20$ km. These results are given in Fig. 4 as a function of target reflectivity. From Figs. 3 and 4, we find that for a system equipped with just an IR camera to achieve an operational range of 20 km and detect a target whose reflectivity is 80%, E_{Tx} must be $\geqslant 0.31$ mJ. For some OPO transmitter systems, this energy requirement is difficult to meet without damaging the crystal and limits the types of glints that can be detected.[4] As a result, in the remainder of this section, three alternative receiver schemes are examined and the minimum energy required for $SNR_D = 1$ determined.

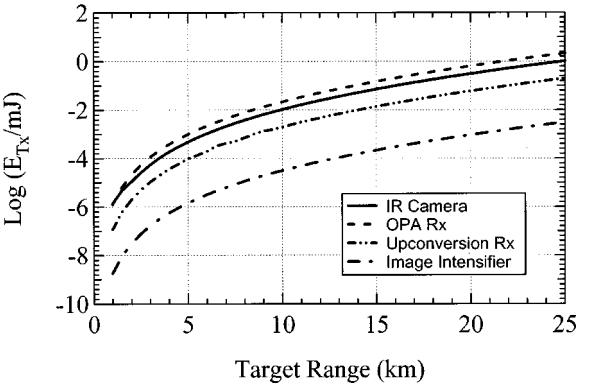

Fig. 3 Minimum transmitted energy required to detect a glint object, with a reflectivity of $\rho = 0.8$, at various target ranges for the IR camera, the OPA, the upconversion, and the image intensifier receivers. Here $SNR_A = 1$ for the OPA receiver and $SNR_D = 1$ for the other receiver designs.

3.1 *OPA Receiver*

One solution for detecting weak returns is to enhance the received signal through a process known as optical parametric amplification (OPA).[15] By placing a separate PPLN crystal, identical to the OPO transmitter, after the receiver aperture and then pumping it with the same wavelength λ_p used in the OPO transmitter, another signal and idler beam will be generated, as before, through DFG. When the incoming light is focused into the crystal, the received signal

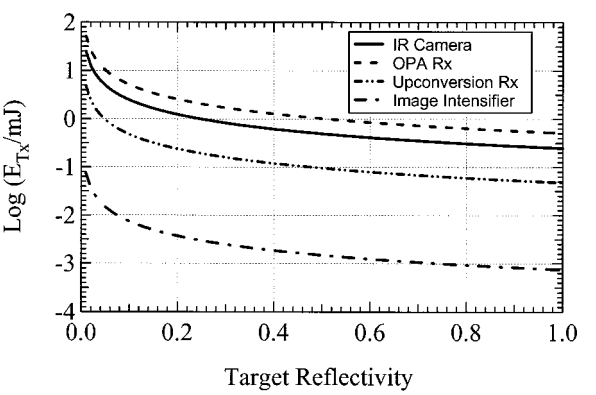

Fig. 4 Minimum transmitted energy versus target reflectivity for the IR camera, the OPA, the upconversion, and the image intensifier receivers at a range of 20 km. Again $SNR_A = 1$ for the OPA receiver and $SNR_D = 1$ for the other receiver designs.

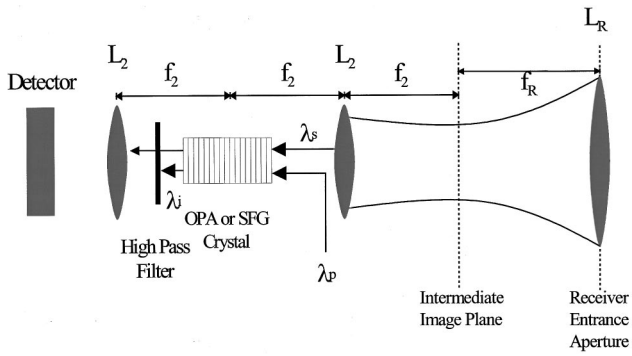

Fig. 5 Modified receiver with an OPA crystal to amplify the glint target return.

coherently stimulates the production of additional signal photons within the OPA, thereby amplifying the glint return. This type of receiver system is depicted in Fig. 5, where each lens L_2 is a coupling optic after the main receiver optic L_R, f_2 is the focal length of the coupling lens, and the distance to the intermediate image plane of the receiver is approximately f_R.

Unfortunately, parametric amplification is not the only process that takes place inside the nonlinear crystal. When the pump beam is incident on the $LiNbO_3$ crystal, spontaneous emission causes a noise term, analogous to that found in electronic amplifiers, to arise within the OPA. The signal and the noise then experience the same gain G across the length of the OPA. If the received power is too weak, the signal-to-noise ratio of the amplifier (SNR_A) will always be less than one, regardless of the pump power. As a result, the parametric noise imposes a lower limit on the amount of energy needed to initially illuminate the glint target.

Since the only requirement for parametric amplification to occur is that $SNR_A \geqslant 1$, the minimum transmitted energy E_{Tx} can be determined from the noise equivalent power (NEP) associated with the DFG interaction between Gaussian beams. Multiplying the photon energy of the signal by the number of thermal photons per mode in a blackbody enclosure, the NEP at the entrance face to the OPA crystal can be written as follows[15]:

$$\mathrm{NEP}=\left(\frac{hc}{\lambda_s}\right)\left(\frac{c}{\lambda_s^2}\right)\Delta\lambda, \tag{11}$$

where h is Planck's constant and c is the speed of light. The spectral acceptance $\Delta\lambda$, centered at the signal wavelength λ_s, may then be determined from the nonlinear efficiency η_{NL} of the DFG process within the PPLN crystal.[3] Assuming that the pump is constant over the entire length of the crystal (i.e., undepleted) and that every incoming photon is amplified, the variation in η_{NL} can be written as[7]

$$\eta_{NL}=\left(1+\frac{\Delta k^2}{4g^2}\right)\sinh^2(gL_c), \tag{12}$$

where g is the following collection of constants:

$$g=\left[\frac{2\pi^2|\chi^{(2)}_{\mathrm{eff}}|^2 I_p}{\lambda_s\lambda_i n_e(\lambda_s,T_c)n_e(\lambda_i,T_c)c\varepsilon_0}-\frac{\Delta k^2}{4}\right]^{1/2}, \tag{13}$$

and I_p is the intensity of the optimally focused pump beam, given by

$$I_p=\frac{2P_p}{\pi\omega_p^2}=\frac{2.84\times 4P_p n_e(\lambda_p,T_c)}{L_c\lambda_p}. \tag{14}$$

Here P_p is the peak pump power, L_c is the crystal length, ε_0 is the permittivity of free space, and $n_e(\lambda_x,T_c)$ is found from the temperature-dependent Sellimer equations describing the extraordinary index of refraction in PPLN.[16] Furthermore, $\chi^{(2)}_{\mathrm{eff}}$ is the effective second-order nonlinear susceptibility tensor element in PPLN, given by[4]

$$\chi^{(2)}_{\mathrm{eff}}=\frac{2}{\pi}\chi^{(2)}_{zzz}=\frac{2}{\pi}(25\ \mathrm{pm/V}). \tag{15}$$

In addition, Δk represents the phase-matching condition between the pump (ω_p), signal (ω_s), and idler (ω_i) frequencies and the crystal grating vector. In PPLN, this interaction can be described, using the conservation of energy as[3]

$$\hbar\omega_s=\hbar\omega_p-\hbar\omega_i, \tag{16}$$

or in terms of the conservation of momentum as

$$\Delta\mathbf{k}=\mathbf{k}_p-\mathbf{k}_s-\mathbf{k}_i-\mathbf{k}_G, \tag{17}$$

where $\hbar=h/2\pi$, and $\mathbf{k}_j$ is the wave vector associated with each field or the crystal grating.

Upon close examination of Eq. (12), we notice that the nonlinear efficiency is essentially dependent on the phase matching $\Delta\mathbf{k}$ buried inside of the g term. For perfect collinear phase matching $\Delta\mathbf{k}=0$. However, as the signal wavelength moves off resonance, the idler wavelength changes to compensate for the variation in photon momentum. This change in $\Delta\mathbf{k}$ can be put in terms of the spectral bandwidth by modifying the conservation of energy and momentum expressions, respectively, as follows:

$$\frac{n_e(\lambda_i,T_c)}{\lambda_i}=\frac{n_e(\lambda_p,T_c)}{\lambda_p}-\frac{n_e(\lambda_s,T_c)}{\lambda_s} \tag{18}$$

and

$$\Delta k=2\pi\left[\frac{n_e(\lambda_p,T_c)}{\lambda_p}-\frac{n_e(\lambda_i,T_c)}{\lambda_i}-\frac{n_e(\lambda_s,T_c)}{\lambda_s}-\frac{1}{\Lambda_G}\right], \tag{19}$$

where Λ_G is the PPLN grating periodicity. Substituting Eqs. (18) and (19) into Eq. (12), the DFG bandwidth can be determined numerically by varying λ_s about its nominal value and defining $\Delta\lambda$ to be the FWHM of the efficiency curve. Using the values $\Lambda_G=31.8\ \mu$m, $T_c=150$°C, $P_p=20$ W, $L_c=25$ mm, $\lambda_p=1.064\ \mu$m, and $\lambda_s=2.1\ \mu$m, the spectral bandwidth is found to be $\Delta\lambda=0.144\ \mu$m. Given this spectral bandwidth, the minimum transmitted energy

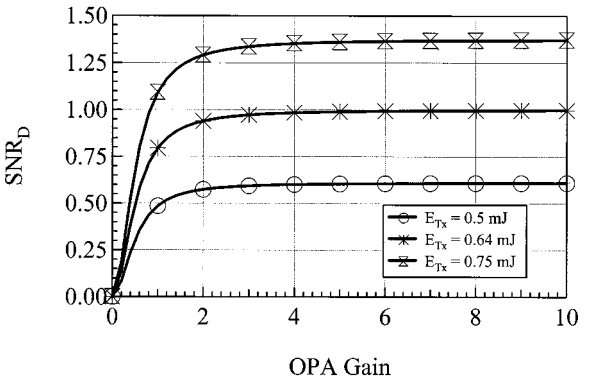

Fig. 6 SNR_D versus the OPA gain at a target range of 20 km. Here $E_{Tx}=0.50$, 0.64, and 0.75 mJ correspond to transmitted powers below, equal to, and above the OPA noise threshold for amplification, respectively.

needed to successfully amplify the glint return is found by setting Eq. (8) equal to the NEP (i.e., $SNR_A=1$) to yield

$$E_{Tx}=\frac{hc^2\,\Delta\lambda\,\Delta\tau}{C\lambda_s^3}, \qquad D_t \leqslant D_{DLS}, \tag{20}$$

where the collection C of constants is again given by Eq. (9). For a ladar system with the design parameters given in Table 1, the minimum transmitter energy needed to overcome the amplifier noise in the OPA receiver is plotted in Fig. 3 for various target ranges and in Fig. 4 for varying target reflectivity at 20 km. From the two figures, we find that the minimum transmitted energy for the OPA receiver is higher than for the IR camera alone. This trend is directly attributed to the large spectral bandwidth associated with the NEP of the nonlinear amplifier. Transmitting a shorter signal wavelength, though, may allow the ladar designer to narrow the spectral acceptance of the OPA crystal. However, due to the eyesafety requirements and the well-defined atmospheric transmission windows,[12] this may prove difficult.

With the minimum signal energy needed to overcome the amplifier noise found, the postdetection signal-to-noise ratio SNR_D can be evaluated and the minimum OPA gain required for successful glint detection can be determined. Multiplying the NEP of the amplifier by the detector responsivity, the signal-to-noise ratio at the detector in terms of the amplifier noise P_{amp} can be written as follows[14]:

$$\begin{aligned}SNR_D&=\frac{P_{sig}}{P_{shot}+P_{thermal}+P_{dark}+P_{amp}}\\&=\frac{(G\mathcal{R}CE_{Tx})^2}{2qG^2\mathcal{R}CE_{Tx}+\dfrac{2k_b\,\Delta\tau\,T_D}{R_L}+2q\,\Delta\tau\,I_D+\left(G\,\Delta\tau\,\mathcal{R}\dfrac{hc^2}{\lambda_s^3}\Delta\lambda\right)^2}.\end{aligned} \tag{21}$$

This expression is very similar to Eq. (9), with the exception of the signal gain G in the numerator and the gain-dependent OPA and shot-noise terms in the denominator. Substituting the system parameters from Table 1 and the IR camera values from Table 2 into Eq. (21), the signal-to-noise ratio can be plotted as in Fig. 6 for a fixed target range of 20 km. Here three different transmitted energies were chosen such that the received energy in Eq. (20) is less than, equal to, and greater than the OPA threshold of $E_{Tx}=0.64$ mJ. When the transmitted energy is just enough to offset the OPA noise, SNR_D approaches one as the amplifier gain increases. Eventually, when the detector gain reaches saturation, the amplifier noise term dominates, and any further gain from the OPA fails to improve the chances of glint detection. From the plot, this minimum OPA gain G for the SNR_D to equal one is only about $G=5$. Moreover, increasing E_{Tx} above the minimum needed to offset the NEP of the amplifier also results in a reduction of the OPA gain threshold. Regardless, both gain values are easily achievable with current OPA technology.[17]

3.2 *Upconversion Receivers*

While the OPA receiver is quite capable of amplifying weak glint signals, it has the major disadvantage that it requires an expensive infrared camera to extract the incoming signal from the target. Furthermore, these cameras often have limited detection bandwidths or numbers of pixels. As a result, they may not be suitable for all airborne ladar systems. One possible solution to these problems is to replace the OPA crystal in Fig. 5 with a new PPLN crystal whose grating periodicity is much smaller. This new crystal is then capable of upconverting the frequency of the incoming signal through sum-frequency generation (SFG).[18] If the upconverted wavelength λ_{sum} then falls within the visible or near IR region of the spectrum, this field can be detected with a silicon CCD array. Not only are CCD cameras much cheaper than IR cameras, they can operate at room temperature as well.

To begin our analysis of such receivers, let us first look at the upconversion process itself. Again using the conservation of energy and momentum, for two collinear fields the SFG interaction can be described by the following two relationships[18]:

$$\hbar\omega_{sum}=\hbar\omega_p+\hbar\omega_s, \tag{22}$$

and

$$\Delta k=2\pi\left[\frac{n_e(\lambda_p,T_c)}{\lambda_p}+\frac{n_e(\lambda_s,T_c)}{\lambda_s}+\frac{1}{\Lambda_G}-\frac{n_e(\lambda_{sum},T_c)}{\lambda_{sum}}\right]. \tag{23}$$

From the conservation-of-energy law in Eq. (22), it is clear that without the presence of a signal photon, the pump photons do not spontaneously upconvert into SFG photons. Ideally then, the upconversion process does not contribute any extra noise to the system. However, in practice this is not the case. Spontaneous noise *has* been observed by Midwinter and Warner in their early experiments with birefringent phase-matched materials.[19] Assuming the angular field of view of the camera is 2π steradians, this upconversion noise P_{upcon} is found by integrating the total spontaneous flux over the detector area, and is expressed as follows[20]:

$$P_{upcon}=\frac{h\omega_{sum}^4\omega_i\omega_R^2P_pL_c|\chi_{eff}^{(2)}|^4}{64\pi c^8\varepsilon_0^2\,\Delta\tau\,n_p^2n_R^2n_{sum}n_iA_c(\Delta k_-)^2}, \tag{24}$$

where A_c is the area of the crystal end face, $\omega_R^2=(\omega_{sum}-\omega_i)^2$, and the phase matching of the collinear downconversion process is given by $\Delta k_-=2k_p+k_G-k_i-k_{sum}$. All other variables denote the same physical parameters as in Eqs. (13)–(15). Additionally, the wavelength and temperature dependence of the index of refraction have been dropped for simplicity, and ω_x denotes the angular frequencies of the various pump, signal, SFG, and DFG idler fields.

Using the above expression for the upconversion noise, the SNR_D of the upconversion receiver can be written as

$$SNR_D = \frac{P_{sig}}{P_{shot}+P_{thermal}+P_{dark}+P_{upcon}} = \frac{(\mathcal{R}\eta_{up}CE_{Tx})^2}{2q\mathcal{R}\eta_{up}CE_{Tx}+\frac{2k_b\Delta\tau T_D}{R_L}+2q\,\Delta\tau I_D+P_{upcon}\Delta\tau^2}, \quad (25)$$

where η_{up} is the efficiency of the upconversion process. As one can see, this expression is very similar to Eq. (21) with the exception of the efficiency term associated with the shot noise and the received signal. Additionally, with the replacement of the OPA by the SFG crystal, there no longer is any system gain. Using Eq. (25) along with $\lambda_i=2.15\ \mu$m and $\lambda_{sum}=706$ nm, the minimum transmitted energy needed to overcome the detector noise can be determined using the system values in Table 1 and the example CCD camera values in Table 2. Setting $SNR_D=1$, the minimum E_{Tx} once again is examined as a function of target range and reflectivity as shown in Figs. 3 and 4, respectively. Note that the idler and SFG wavelengths were obtained by solving the conservation-of-energy relationships for the DFG and SFG interactions given in Eqs. (11) and (22), respectively, for an ideal upconversion efficiency of $\eta_{up}=100\%$ (i.e., every signal photon produces a SFG photon). We also assume a $25\times15\times1$-mm PPLN crystal poled at 15.9 μm, pumped with 20 W, and operated at a temperature $T_c=100°$C. From Figs. 3 and 4, we see that in the absence of the amplifier noise, at all ranges and reflectivities, the minimum energy requirement is nearly an order of magnitude less than that needed for the OPA system or IR camera discussed earlier. Thus, replacing the IR detector with a visible CCD camera does lower the minimum energy and allows the operator to use a technology that is generally more stable, more compact, and much cheaper than most IR cameras.

3.3 *Image Intensifier Receiver*

In an additional effort to incorporate the CCD camera into the receiver system, the last ladar system investigated is an upconversion receiver incorporating an image intensifier. Under low light conditions, a small amount of radiation from the target, incident on the front surface of the device, is amplified by a series of photocathodes.[21] The primary advantage of the image intensifier is that it can easily have an optical gain on the order of 100,000.[22] With such a dramatic increase in signal power, the image intensifier is ideally suited for enhancing the glint return. Until recently

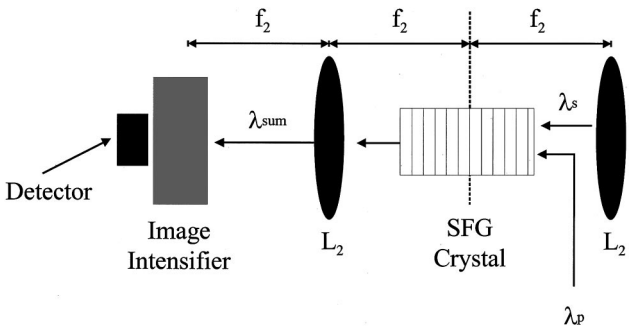

Fig. 7 Diagram of the image intensifier receiver system. The incoming signal is upconverted to a visible wavelength and then amplified by an image intensifier before being detected.

though, most photocathodes have been restricted to submicron wavelengths.[23] Therefore, upconversion to visible wavelengths is needed to detect the IR signal over a wide band.[24] Except for a slight modification, the image intensifier system shown in Fig. 7 is very similar to the upconversion receiver in Sec. 3.2. As before, the glint signal is collected and Fourier transformed into the upconversion crystal where it is upconverted. The resulting signal is then imaged onto an image intensifier before being detected by the CCD array.

Given the image intensifier receiver, the SNR_D for the system can now be calculated. Since the photocathode gain across the device is not uniform, the output current and thus the noise of the system are also no longer constants. This deviation in photocurrent can be accounted for by finding the mean $\langle i\rangle$ and the variance σ_i^2 of the output current as a function of the mean random gain $\overline{G}$. By averaging over all the random events *and* random gains associated with the image intensifier, it can be shown that the mean output current *and* the variance are given by[25]

$$\langle i\rangle=\overline{i}=\frac{q\overline{G}P_R\eta_{QE}}{h\nu}=\overline{G}P_R\mathcal{R} \quad (26)$$

and

$$\sigma_i^2=\frac{2q^2\overline{G}^2\eta_{QE}B_wFP_R}{h\nu}=\frac{2q\overline{G}^2FP_R\mathcal{R}}{\Delta t}, \quad (27)$$

where q is the charge of the electron, η_{QE} is the quantum efficiency, B_w is the bandwidth, and F is the noise figure associated with the image intensifier.

Using Eqs. (25) and (26), the signal-to-noise ratio at the detector for the image intensifier receiver is given by

$$SNR_D=\frac{P_{sig}}{P_{shot}+P_{thermal}+P_{dark}+P_{upcon}} = \frac{(\overline{G}\mathcal{R}\eta CE_{Tx})^2}{2q\mathcal{R}\eta F\overline{G}^2CE_{Tx}+\frac{2k_b\Delta\tau T_D}{R_L}+2q\,\Delta\tau I_D+\Delta\tau^2 P_{upcon}}, \quad (28)$$

where P_{upcon} is given by Eq. (24). Note that the quantum efficiency η associated with the received power is the product of the upconversion efficiency and the quantum efficiency of the photocathodes inside the image intensifier. While this expression is in many respects similar to Eq. (25), several differences need to be highlighted. Unlike the OPA receiver, the mean gain for the image intensifier is not a function of the pump power or crystal properties. Once a specific device is chosen, the mean gain across the device is fixed and measurable. As mentioned earlier, this gain can be as high as 100,000. The noise power factor F is also quantifiable, by measuring the SNR before and after the device: the ratio of the input SNR to the output SNR is F.[25] For most second- and third-generation devices, the value of F ranges from 3 to 5.

With the mean gain now constant, the minimum transmitted power from the OPO can readily be determined. Assuming a conservative gain of 20,000 and $F=4$, the signal-to-noise ratio can be evaluated in conjunction with the values in Tables 1 and 2. Substituting these values into Eq. (27), the minimum E_{Tx} is calculated as a function of target range and reflectivity as before, and is illustrated in Figs. 3 and 4. In comparison with the other systems in Fig. 3, the minimum energy requirement for the image intensifier system is two orders of magnitude lower. Thus this system allows one to take advantage of the wide tunability of the OPO transmitter while providing the best chance of detecting single glint targets in an ideal environment.

4 Conclusions

Ladar systems currently under investigation incorporating periodically poled lithium niobate in the transmitter can have an operating range anywhere from 1.1 to 5.5 μm if several grating structures are poled onto a single piece of PPLN. This wide tunability makes the OPO-based system very attractive for multispectral target interrogation. Unfortunately, detecting such a wide range of IR signals often requires a significant amount of transmitted energy. OPO transmitters, though, are inherently limited in the amount of power available for target illumination and thus have a restricted range of operation. However, the contrast offered by glint returns over diffuse returns can be used with the appropriate system parameters to allow for selective detection of glint and not the background. Assuming a typical system geometry and some reasonable detector characteristics, this paper has presented four receiver designs for detecting glint returns. Each design was then evaluated by setting the receiver SNR detection threshold equal to one and using the minimum transmitted energy as the figure of merit.

Through numerical analysis, we have shown that parametric amplification of glint returns before detection has roughly the same energy requirements as the IR camera alone. These two receiver schemes both incorporate an expensive IR camera and are difficult to operate on airborne platforms. To overcome such limitations, a similar receiver design involving image upconversion was also investigated. By upconverting the frequency of the incoming light to the near IR region of the spectrum, not only is it possible to use a cheaper and more reliable CCD camera, but the minimum transmitted energy may be decreased by nearly an order of magnitude.

The last design involved an image intensifier to enhance the upconverted signal before detection with a CCD. Assuming a trivial device gain of 20,000, the minimum energy needed for detection was lowered by an additional two orders of magnitude from that of the OPA receiver. However, while the image-intensifier receiver has the lowest energy requirements and provides the greatest chance of detecting glint targets against a diffuse background, it may often be too sensitive for most airborne systems. For example, if a genuine glint target is located in a desert environment, random glint returns from the sand may be enough to trigger the detector, thereby causing the target to be lost in background clutter. Therefore, while the image intensifier receiver may have the lowest transmitted energy requirements of the four receiver designs, the upconversion receiver may provide the best possibility of detecting desired glint targets without being subject to false alarms.

References

1. J. A. Overbeck, M. B. Mark, S. H. McCracken, P. F. McManamon, and B. D. Duncan, "Coherent versus incoherent ladar detection at 2.09 mm," *Opt. Eng.* **32**(11), 2681–2689 (1993).
2. H. Hasson, R. Wendt, and S. R. Czyzak, "Overview of the field ladar demonstration program developing high-resolution imaging and remote sensing," in *Laser Radar Technology and Application*, G. W. Kamerman, Ed., *Proc. SPIE* **2748**, 294–308 (1996).
3. R. W. Boyd, *Nonlinear Optics*, Academic Press, San Diego, CA (1992).
4. L. E. Myers, R. C. Eckardt, M. M. Fejer, and R. L. Byer, "Quasi-phase-matched optical parametric oscillators using bulk periodically poled lithium niobate," *J. Opt. Soc. Am. B* **12**(11), 2102–2116 (1995).
5. L. E. Myers, R. C. Eckardt, M. M. Fejer, and R. L. Byer, "Multigrating quasi-phase-matched optical parametric oscillators in periodically poled $LiNbO_3$," *Opt. Lett.* **21**(8), 591–593 (1996).
6. R. L. Byer, "Optical parametric oscillators," in *Quantum Electronics: A Treatise*, H. Rabin and C. L. Tang, Eds., pp. 587–597, Academic Press, New York (1975).
7. M. S. Salisbury, P. F. McManamon, and B. D. Duncan, "Sensitivity improvement of a 1 μm ladar system incorporating an optical fiber preamplifier," *Opt. Eng.* **32**(11), 2671–2680 (1993).
8. A. V. Jelalian, *Laser Radar Systems*, Artech, Boston (1992).
9. O. Steinvall, "Effects of target shape and reflection on laser radar cross-sections," *Appl. Opt.* **39**(24), 4381–4391 (2000).
10. J. H. Shapiro, "Target-reflectivity theory for coherent laser radars," *Appl. Opt.* **21**(18), 3398–3408 (1982).
11. R. W. Boyd, *Radiometry and the Detection of Optical Radiation*, Wiley, New York (1983).
12. G. C. Holst, *Electro-optical Imaging System Performance*, 2nd ed., SPIE Optical Engineering Press, Bellingham, WA (2000).
13. J. W. Goodman, *Introduction to Fourier Optics*, 2nd ed., McGraw-Hill, New York (1996).
14. J. A. Overbeck, M. S. Salisbury, M. B. Mark, and E. A. Watson, "Required energy for a laser radar system incorporating a fiber amplifier or an avalanche photodiode," *Appl. Opt.* **34**(33), 7724–7730 (1995).
15. D. C. Hanna, M. A. Yuratich, and D. Cotter, *Nonlinear Optics of Free Atoms and Molecules*, Springer-Verlag, Berlin (1979).
16. D. H. Jundt, "Temperature-dependent Sellmeier equation for the index of refraction, n_e, in congruent lithium niobate," *Opt. Lett.* **22**(20), 1553–1555 (1997).
17. M. J. Missey, V. Dominic, and P. E. Powers, "Periodically poled lithium niobate monolithic nanosecond optical parametric oscillators and generators," *Opt. Lett.* **24**(17), 1227–1229 (1999).
18. P. Gunter, *Nonlinear Optical Effects and Materials*, Springer-Verlag, Berlin (2000).
19. J. E. Midwinter and J. Warner, "Upconversion of near infrared to visible radiation in lithium-meta-niobate," *J. Appl. Phys.* **38**(2), 519–535 (1967).
20. C. L. Tang, "Spontaneous emission in the frequency upconversion process in nonlinear optics," *Phys. Rev.* **182**(2), 367–374 (1969).
21. I. P. Csorba, "Image intensifiers," *Inf. Disp.*, pp. 16–19 (Jan. 1990).
22. J. Dupuy, J. Schijvers, and G. Wolzak, "The super second generation image intensifier," *Proc. SPIE* **1072**, 13–18 (1989).
23. V. Aebi and P. Vallianos, "Laser-illuminated viewing provides long-range detail," *Laser Focus World* **36**(9), 147–150 (2000).
24. B. E. A. Seleh and M. C. Teich, *Fundamentals of Photonics*, Wiley, New York (1991).
25. C. Ciamberlini, G. Longobardi, P. L. Ramazza, and S. Residori, "New

approach to noise factor measurements of imaging devices,'' *Opt. Eng.* **33**(3), 845–848 (1994).

Christopher D. Brewer received a BS degree in physics from Marshall University in 1995. He then went on to obtain a MS degree in 1997, and subsequently a PhD in 2001, from the University of Dayton in electro-optics, while working as a research assistant at Wright Patterson Air Force Base. Currently, he is a member of the University of Dayton Research Institute, where he is actively involved with the Electro-Optic Sensors Group of the Air Force Research Laboratory, pursuing agile beamsteering applications of both liquid-crystal devices and microlens arrays. Other research interests include nonlinear optics and materials, ladar imaging, and glint target tracking.

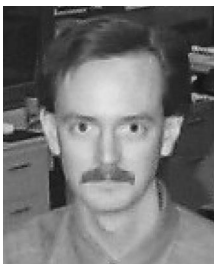

Bradley D. Duncan moved to Dayton, OH, in August of 1991 after receiving the PhD degree in electrical engineering from Virginia Polytechnic Institute and State University (Virginia Tech). Upon arriving in Dayton he joined the University of Dayton (UD) faculty, where he is now a tenured (full) professor of electrical and computer engineering, with a joint appointment in the graduate electro-optics program. Dr. Duncan's research interests and activities span a wide range of areas within the optical sciences, including the study of ladar systems, photorefractive applications, fiber optic sensor and system technology, integrated optics, nondestructive evaluation, and scanning and nonlinear optical image processing. Dr. Duncan is a member of the OSA, SPIE, and ASEE. He is also a senior member of the IEEE. He has previously served as the book reviews editor for *Optical Engineering* (the international journal of SPIE), and is the faculty advisor for both the University of Dayton student chapter of the OSA, and EΔT—UD's engineering social fraternity. Dr. Duncan directs the research conducted in the UD's NSF Photonics Laboratory, and in 1998 won the Engineering Best Professor of the Year award.

Edward A. Watson is the technical advisor for the Electro-Optical Technology Division, Sensors Directorate, Air Force Research Laboratory. He conducts research in active and passive electro-optic sensors, including the application of dynamic diffractive optical components to the agile steering and shaping of monochromatic and polychromatic light beams, development of multiphenomenology laser radar imagers, and modeling of aliasing and blurring in sampled imagery. He has a PhD in optics from the University of Rochester, and an MS in optical sciences and a BS in physics from the University of Arizona.